Phase separation, interface properties, and charge density waves in a simplified model for a macroion suspension

Patrick B. Warren
Unilever R&D Port Sunlight, Bebington, Wirral, CH63 3JW, United Kingdom
(Received 22 June 2005; revised manuscript received 21 December 2005; published 26 January 2006)

A simplified density functional theory for a macroion suspension is examined, where the correlation free energy corresponds to the macroion self-energy, treated within a linearized or Debye-Hückel approximation. The model possesses a miscibility gap (liquid-liquid phase separation) at low ionic strength. Within the gap, density profiles, electrical structure, and surface tension are calculated for the interface between coexisting phases, using a variational approximation. Additionally, structure factors are calculated for the homogeneous system. As one approaches the critical points, the structure factors can diverge at a nonzero wave vector, signaling the onset of charge density wave phases. Although the quantitative results should be treated with care, the results may be indicative of the rich phenomenology that can arise in asymmetric charged systems.

DOI: 10.1103/PhysRevE.73.011411 PACS number(s): 82.70.Dd, 05.20.Jj, 05.70.−a, 64.75.+g

I. INTRODUCTION

The phase behavior of macroion suspensions has attracted much interest over the last decade. There is a plethora of sometimes conflicting experimental and theoretical results, and several reviews are available [1–5]. Simulations have clearly shown that liquid-liquid phase separation occurs in a macroion suspension at strong enough electrostatic coupling [6–10], corresponding to a multivalent supporting electrolyte and/or a reduced dielectric constant. Where phase separation occurs, outstanding questions remain about the density profiles, surface tension, and electrical structure of the interfacial region between the coexisting phases. These questions provide the focus of the present paper.

The approach to these issues taken here is to develop a density functional theory (DFT), motivated by the earlier analysis in Ref. [11] (see also Appendix A). To make progress, a rather gross simplification has been adopted, in which the *only* contribution to the correlation free energy in the DFT arises from the macroion self-energy computed in a simple closed form using Debye-Hückel theory. The reasons for studying such a simplified model are threefold. First, although the model is very basic, it nevertheless possesses a rich and perhaps surprising phenomenology which may be relevant to the study of real systems. Second, the starting point is sufficiently simple that a physically motivated ansatz to a DFT can be written down "by inspection." Third, there are very few examples of the application of DFT to *asymmetric* charged systems and the present analysis reveals some interesting technical points which may be transferrable to more complicated and more realistic models.

It is crucial for internal consistency that the DFT used to solve for the interfacial properties and structure factors is also used to generate the bulk phase behavior. Fortunately, when applied to a homogeneous system, the present DFT describes phase separation in the form of a miscibility gap at low ionic strength which is in reasonable accord with more sophisticated approaches. The physics of the phase separation lies in the dependence of the macroion self-energy on the local ionic strength: macroions drift toward regions of high ionic strength, which by charge neutrality are regions where other macroions have also congregated. This is a many-body effect. Within the linearization approximation, the effect grows without bound as the macroion charge is increased, and thus the mechanism can drive phase separation at sufficiently large macroion charges. In reality, nonlinear effects (counterion condensation) limit the effective macroion charge [12–16], and therefore this mechanism is likely insufficient in itself to drive phase separation in real systems [17–23]. It is still a contributing factor in real systems though, operating in conjunction with other effects such as correlated fluctuations in the counterion clouds around macroions and the sharing of counterions between macroions [6,7,9,24,25] (see also Appendix B). In the context of the present model, phase separation is found in a region in parameter space where the neglected nonlinear effects should start to become important. Therefore, one should interpret the quantitative results with caution.

The results obtained for the density profiles and the surface tension between coexisting phases are in accord with previous expectations, and include the appearance of a liquid-liquid junction potential [11,26–28]. In addition, the model also makes predictions for the structure factors. These are found to obey the Stillinger-Lovett moment conditions [29,30], although it turns out this is not a stringent test of the theory. Surprisingly, the structure factors may diverge at a nonzero wave vector as one approaches the critical points. This suggests the possibility that the critical points in these systems may be replaced by charge density wave phases [31]. This phenomenological possibility in charged systems was first suggested by Nabutovskii and co-workers [32–34].

The only previous work on the interfacial properties of a phase-separated macroion suspension appears to be that of Knott and Ford [35]. They compute the surface tension using square-gradient theory, but discard the possible electrical structure at the interface.

II. SPECIFICATION OF THE MODEL

The model treats macroions as spheres of (positive) charge Z, diameter σ, and number density ρ_m (volume frac-

tion $\phi=\pi\sigma^3\rho_m/6$). Also present are small ions ("salt" ions) which are univalent counterions and coions at number densities ρ_- and ρ_+, respectively. It is supposed that there is only one species of counterion. All the ions are embedded in a structureless dielectric continuum characterized by a Bjerrum length l_B, so that the electrostatic interaction energy between a pair of univalent charges separated by a distance r is l_B/r, in units of k_BT where k_B is Boltzmann's constant and T is the temperature (for water at room temperature, $l_B\approx 0.72$ nm). Assuming that the size of the small ions is irrelevant (see Appendix C), the interactions are thus completely parametrized by the dimensionless ratio σ/l_B and the charge Z. It is often convenient to pretend that the dielectric permittivity of the background is independent of temperature, in which case $l_B\sim 1/T$. This means that σ/l_B can be regarded as a dimensionless temperature.

The DFT is specified by giving the free energy F as a functional of the spatially varying number densities $\rho_m(\mathbf{r})$ and $\rho_\pm(\mathbf{r})$ [36,37]. The functional is decomposed into ideal, mean-field, and correlation contributions:

$$\frac{F}{k_BT}=\int d^3\mathbf{r}\sum_{i=m,\pm}\rho_i(\mathbf{r})\ln\frac{\rho_i(\mathbf{r})}{e\rho_i^0}+\frac{l_B}{2}\int d^3\mathbf{r}\,d^3\mathbf{r}'\frac{\rho_z(\mathbf{r})\rho_z(\mathbf{r}')}{|\mathbf{r}-\mathbf{r}'|}+\frac{1}{k_BT}\int d^3\mathbf{r}\,\rho_m(\mathbf{r})f_m(\mathbf{r}). \tag{1}$$

The first term is the ideal term, where e is the base of natural logarithms and the ρ_i^0 are unimportant base units of concentration related to the definition of the standard state [38]. The second term is a mean-field electrostatics term, where $\rho_z(\mathbf{r})=\Sigma_i z_i\rho_i(\mathbf{r})$ is the local charge density, with $z_i=\{Z,1,-1\}$ as $i=\{m,+,-\}$, and a factor $1/2$ to allow for double counting. The third term represents the correlation free energy. As discussed in the Introduction, only the macroion self-energy f_m is included in this term. This is computed using Debye-Hückel theory [39–42],

$$f_m(\mathbf{r})=\frac{2Z^2l_Bk_BT}{\sigma[\sigma\kappa(\mathbf{r})+2]}, \tag{2}$$

where $\kappa(\mathbf{r})$ is a local inverse Debye screening length, defined in terms of an *average* local ionic strength $\bar{\rho}_I(\mathbf{r})$ through

$$[\kappa(\mathbf{r})]^2=8\pi l_B\bar{\rho}_I(\mathbf{r}),$$

$$\bar{\rho}_I(\mathbf{r})=\int d^3\mathbf{r}'w(|\mathbf{r}-\mathbf{r}'|)\rho_I(\mathbf{r}'),$$

$$\rho_I(\mathbf{r}')=[\rho_+(\mathbf{r}')+\rho_-(\mathbf{r}')]/2. \tag{3}$$

The ionic strength includes all the small ions, but not the macroions [11]. In principle, allowance could be made for the macroion excluded volume, but this effect is of secondary importance and for simplicity has been omitted.

The smoothing kernel in Eqs. (3) is normalized so that $\int d^3\mathbf{r}\,w(r)=1$. Most of the analysis below has been carried out with the arbitrary choice [43]

$$w(r)=(\pi\alpha\sigma^2)^{-3/2}\exp[-r^2/(\alpha\sigma^2)]. \tag{4}$$

This smoothing kernel is of range $\sigma\sqrt{\alpha}$. The argument below suggests that the parameter α should be of order unity. For the most part therefore I will set $\alpha=1$ in the calculations. Equations (1)–(4) completely specify the DFT, and everything discussed below can be derived from them.

The decomposition into ideal, mean-field, and correlation contributions is a standard approach [44–48]. The approximation made for the correlation term deserves more discussion though. As discussed in the Introduction, the only piece of physics that has been incorporated is the macroion self-energy. This has a nontrivial dependence on the local ionic strength since each macroion polarizes the surrounding electrolyte and becomes surrounded by a "double layer." The polarization is obviously a local effect though, which allows for a straightforward ansatz to be made for the correlation contribution in a spatially inhomogeneous system, as indicated in Eqs. (1)–(4). The unobvious step is the requirement to introduce some notion of smoothing, or smearing, in the sampling of the local ionic strength. The physical motivation for this is that one can derive the self-energy by integrating out the small ion degrees of freedom, with the main contribution coming from variations on length scales corresponding to the structure in the double layer [40]. Thus only variations in ionic strength on length scales $\gtrsim\sigma$ should be included in the model. The smoothing kernel is a device for achieving this (and motivates the choice for α). A second technical reason for introducing the smoothing kernel is found below in Sec. V. The DFT becomes unphysical with respect to the structure factors if one uses a "point model" where the dependence is on the ionic strength at, say, the center of the macroion.

The potential energy of a small ion at the surface of the macroion, in units of k_BT, is $\pm Zl_B/\sigma$. Equation (2) uses the Debye-Hückel expression for the self-energy, which assumes Zl_B/σ is small. The expression becomes increasingly inaccurate for $Zl_B/\sigma\gtrsim 1$ [17–23]. The interesting effects are found only at larger values of Zl_B/σ though, where nonlinear effects start to become important. Therefore, as already mentioned, one should treat the quantitative results with caution.

III. BULK PHASE BEHAVIOR

In this section, I shall consider the bulk phase behavior predicted by the free energy of Eqs. (1)–(4). This is a homogeneous situation in which the density variables lose their spatial dependence. In this limit, one can prove that the mean field term should be replaced by a condition of bulk charge neutrality, $\rho_z=\Sigma_i z_i\rho_i=0$ [19,49].

The required charge neutrality condition can be imposed in two ways. The first route is to add a term $\psi k_BT\Sigma_i z_i\rho_i$ to the free energy, where ψk_BT is a Lagrange multiplier. This approach has the advantage of making a close connection to the DFT. Taking this approach, the free energy becomes

$$\frac{F}{Vk_BT}=\sum_i\rho_i\left(\ln\frac{\rho_i}{e\rho_i^0}+z_i\psi\right)+\frac{2Z^2l_B\rho_m}{\sigma(\sigma\kappa+2)} \tag{5}$$

where V is the system volume and $\kappa^2=4\pi l_B(\rho_++\rho_-)$. The distinction between the smoothed and unsmoothed ionic

strengths disappears in the homogeneous limit. In this approach the ρ_i are treated as three independent density variables. At the end of any calculations, ψ is adjusted to get $\Sigma_i z_i \rho_i = 0$. The value of ψ depends on the state point under consideration.

The second way to enforce charge neutrality is to eliminate one of the density variables. Since this is numerically quite convenient, it is the approach that will be adopted in the rest of this section. Following convention, one writes $\rho_- = Z\rho_m + \rho_s$ and $\rho_+ = \rho_s$, where ρ_s is the added salt concentration. Substituting for $\rho_\pm$ in Eq. (5) gives a free energy from which ψ has disappeared, and which depends only on two independent density variables ρ_m and ρ_s.

I now discuss the phase behavior predicted by this free energy. First, in the absence of salt some additional simplifications can be made. In the limit $\rho_s \to 0$, the free energy can be written in a dimensionless form as

$$\frac{1}{Z}\frac{\pi\sigma^3 F}{6Vk_BT} = \phi \ln \phi + \frac{u}{\sqrt{6u}+1} \tag{6}$$

where $u = \phi Z l_B/\sigma$ and ϕ is the macroion volume fraction. To get to this point, I have assumed that $Z \gg 1$ and hidden some constants and terms strictly proportional to ρ_m since they do not affect the phase behavior.

Equation (6) predicts that the dependence on σ/l_B and Z is through the single combination Zl_B/σ (there is no reason to suppose that this should be the case in a more accurate theory). This is the same parameter that quantifies the accuracy of the Debye-Hückel linearization approximation. The inverse of this, $\sigma/(Zl_B)$, is proportional to the dimensionless temperature discussed above. Figure 1(a) shows the universal phase behavior predicted by Eq. (6) as a function of the macroion volume fraction and $\sigma/(Zl_B)$. At small enough values of $\sigma/(Zl_B)$, a two-phase region is encountered in the phase diagram. The two-phase region corresponds to phase coexistence between macroion-rich and macroion-poor phases. The identities of these phases merge at a critical point located at $\phi \approx 9.18 \times 10^{-3}$ and $\sigma/(Zl_B) \approx 0.132$.

One can compare this with the simulation results of Reščič and Linse for $Z=10$ macroions [10] (see also Appendix B). They also find a two-phase region on lowering temperature, with a critical point located at $\phi \approx 0.15$ and $\sigma/(Zl_B) \approx 0.077$. While the phenomenology is the same, the numerical values are somewhat different from the prediction of Eq. (6). Not unexpectedly, the present model is too crude to obtain quantitatively reliable results. Interestingly, in terms of accuracy of prediction, the present theory is not much worse than symmetrized Poisson-Boltzmann theory or the mean spherical approximation [50–52].

I now turn the effect of added salt, and analyze the predictions of the full free energy in Eq. (5). In general, as salt is added, the critical point in Fig. 1(a) first moves to higher dimensionless temperatures, passes through a maximum, and then starts to move to lower dimensionless temperatures again. This nonmonotonic behavior is shown in Fig. 1(b) for $Z=10^3$. A similar effect of added salt is seen in a number of other approaches [11,20,21,39,40,53], although interestingly it is contradicted by a recent simulation study [54]. This

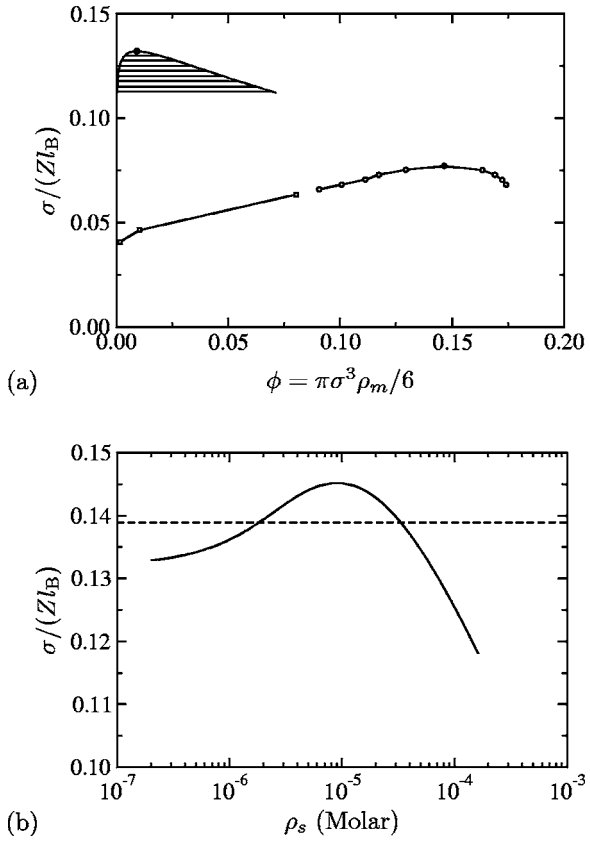

FIG. 1. (a) Universal phase behavior in the absence of salt, predicted by Eq. (6) (upper curve). The simulation results of Reščič and Linse [10] are also shown (lower curve with marked points). (b) Behavior of the critical point at $Z=10^3$ as salt is added. The dashed line corresponds to the parameters used in Fig. 2 below.

difference might be related to the assumed size of the small ions though, as discussed in Appendix C. In the presence of added salt, it is no longer true that the dependence on Z and σ/l_B can be combined into a single parameter; however, for comparison with the phase behavior in the absence of salt, Fig. 1(b) shows the behavior as a function of $\sigma/(Zl_B)$ at this fixed value of Z.

The reentrant behavior means that for parameters such as those corresponding to the dashed line in Fig. 1(b), there are *two* critical points in the (ρ_m, ρ_s) plane, and one encounters a reentrant single-phase region at low added salt. The dashed line in Fig. 1(b) is for $Z=10^3$, $\sigma=100$ nm, and $l_B=0.72$ nm, and the corresponding phase behavior in the (ρ_m, ρ_s) plane is shown in Fig. 2. It is seen that the two phase region appears as a miscibility gap in this representation.

As σ/l_B is increased or Z is decreased, the two critical points move towards each other and finally disappear at a double critical point, or hypercritical point [55]. For example, for $Z=10^3$ the double critical point corresponds to the maximum of the solid line in Fig. 1(b), where $\sigma/(Zl_B) \approx 0.145$, $\phi \approx 1.04 \times 10^{-2}$, and $\rho_s \approx 8.98$ μM.

The bulk phase behavior predicted by the homogeneous version of the DFT, Eq. (5), thus closely resembles that predicted by various other approaches including the theory discussed in Ref. [11].

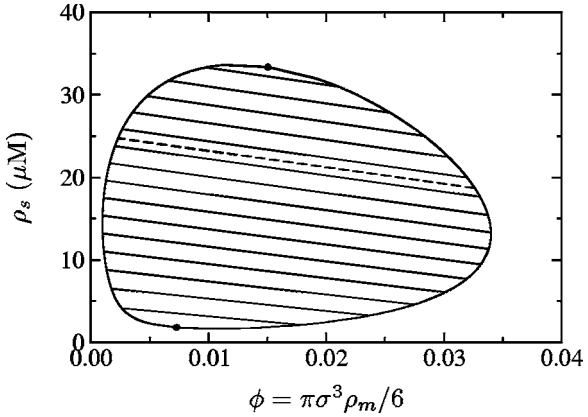

FIG. 2. Phase behavior at $Z=10^3$, $\sigma=100$ nm, and $l_B=0.72$ nm, corresponding to the dashed line in Fig. 1. The miscibility gap is bounded above and below by critical points. The dashed tie line is the one for which the interfacial properties are reported in Figs. 3–5 below.

IV. INTERFACIAL PROPERTIES

The reason for introducing the DFT, of course, is to calculate the macroion and small ion density profiles through the interface between two coexisting phases, and to compute the surface tension. In order to set the problem up, it is convenient to introduce the grand potential [36,37]

$$\Omega = F - \int d^3\mathbf{r} \sum_{i=m,\pm} \mu_i \rho_i(\mathbf{r}) \tag{7}$$

where μ_i are the chemical potentials of the three species, and F is defined in Eqs. (1)–(4). At this point it is also convenient to rewrite the mean-field term in Eq. (1). Define a dimensionless electrostatic potential

$$\psi(\mathbf{r}) = l_B \int d^3\mathbf{r}' \frac{\rho_z(\mathbf{r}')}{|\mathbf{r}-\mathbf{r}'|} \tag{8}$$

so that the mean-field term in Eq. (1) can be written

$$\frac{l_B}{2} \int d^3\mathbf{r}\, d^3\mathbf{r}' \frac{\rho_z(\mathbf{r})\rho_z(\mathbf{r}')}{|\mathbf{r}-\mathbf{r}'|} = \frac{1}{2} \int d^3\mathbf{r}\, \psi(\mathbf{r})\rho_z(\mathbf{r}). \tag{9}$$

By direct substitution, one verifies that the potential defined by Eq. (8) solves the Poisson equation

$$\nabla^2\psi + 4\pi l_B \rho_z = 0. \tag{10}$$

Using this and Green's first identity [56], the mean-field term now becomes

$$\frac{1}{2} \int d^3\mathbf{r}\, \psi(\mathbf{r})\rho_z(\mathbf{r}) = \frac{1}{8\pi l_B} \int d^3\mathbf{r} |\nabla\psi|^2. \tag{11}$$

This is recognized as the electric field energy since $\nabla\psi$ is essentially the electric field strength. One can now define a grand potential density $\omega(\mathbf{r})$ such that $\Omega=\int d^3\mathbf{r}\, \omega(\mathbf{r})$ and

$$\omega = \sum_i \rho_i \left(k_B T \ln \frac{\rho_i}{e\rho_i^0} - \mu_i \right) + \frac{k_B T}{8\pi l_B} |\nabla\psi|^2 + f_m \rho_m \tag{12}$$

where the explicit dependence on the spatial coordinate has been suppressed. For a homogeneous system, $\omega=-p$ where p is the pressure.

Setting $\delta\Omega/\delta\rho_i(\mathbf{r})=0$ and using Eq. (8) gives

$$\frac{\mu_i}{k_B T} = \ln \frac{\rho_i(\mathbf{r})}{\rho_i^0} + z_i\psi(\mathbf{r}) + \frac{\delta}{\delta\rho_i(\mathbf{r})} \left(\frac{\int d^3\mathbf{r}'\, \rho_m(\mathbf{r}') f_m(\mathbf{r}')}{k_B T} \right). \tag{13}$$

I now suppose that all the variation occurs in one direction x normal to the interface. At large distances from the interface, $x\to\pm\infty$, the number densities approach those corresponding to the coexisting bulk phases. The grand potential density approaches a constant value $\omega(\pm\infty)$ equal to (minus) the pressure, and therefore the same in coexisting phases. The surface tension γ can therefore be identified as the excess grand potential per unit area

$$\gamma = \int_{-\infty}^{\infty} dx [\omega - \omega(\pm\infty)]. \tag{14}$$

To make a connection with the bulk phase behavior, consider the chemical potentials as derived from Eq. (5),

$$\frac{\mu_i}{k_B T} = \ln \frac{\rho_i}{\rho_i^0} + z_i\psi + \frac{\partial}{\partial\rho_i} \left(\frac{2Z^2 l_B \rho_m}{\sigma(\sigma\kappa+2)} \right). \tag{15}$$

Comparison with Eq. (13) shows that ψ in Eq. (5) is simply the limiting value of $\psi(\mathbf{r})$ in Eq. (13), in the case of a homogeneous system [57].

For the interface problem, one has two limiting values $\psi(\pm\infty)$, which are not the same. The difference $\Delta\psi=\psi(\infty)-\psi(-\infty)$ arises because of the electrical structure at the interface. It is a liquid-liquid junction potential analogous to the Donnan potential that appears across a semipermeable membrane [58,59]. Since ψ in Eq. (15) is determined by the bulk densities, the difference $\Delta\psi$ can be calculated without having to solve for the interface structure. In fact, because of the symmetric way that $\rho_\pm$ enters into the correlation free energy, a simple expression obtains [11],

$$\Delta\psi = \frac{1}{2} \ln \left(\frac{\rho_-(\infty)}{\rho_+(\infty)} \frac{\rho_+(-\infty)}{\rho_-(-\infty)} \right). \tag{16}$$

What should be used for the chemical potentials though? Note first that global charge neutrality means Eq. (14) for the surface tension is unaffected by a global shift in ψ. Hence we are free to set $\psi=0$ in one of the coexisting phases. Then Eq. (15) with $\psi=0$ and bulk densities corresponding to the chosen reference phase fixes the chemical potentials (the ρ_i^0 dependence will cancel out). For the inhomogeneous problem this means one can take, for example, $\psi(-\infty)=0$ with $\rho_i(-\infty)$ corresponding to the bulk densities in the chosen reference phase, and $\psi(\infty)=\Delta\psi$ computed from Eq. (16), with $\rho_i(\infty)$ corresponding to the bulk densities in the phase that coexists with the chosen reference phase.

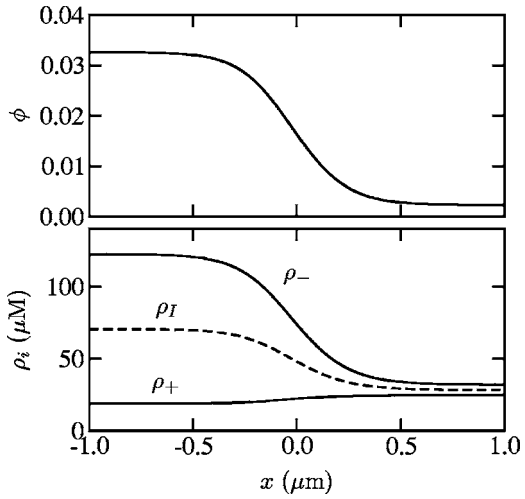

FIG. 3. Macroion volume fraction (top) and small ion concentrations (bottom) through the interface corresponding to the dashed tie line in Fig. 2.

In principle, at this point the nonlinear integral equations should be solved together with the Poisson equation to find the ion density profiles. Alternatively, a variational approximation can be adopted in which γ is minimized with respect to parameters in trial functions which specify the ion density profiles. The trial functions can be chosen to satisfy the required boundary conditions automatically. This variational alternative is the one that has been followed in the present work, and more details of the numerical approach are given in Appendix D.

I now turn to the results. Figure 3 shows representative density profiles for the macroion and small ions through the interface between the coexisting phases, corresponding to the highlighted tie line in Fig. 2. The profiles interpolate smoothly between the coexisting bulk densities. Figure 4 shows the detailed electrical structure at the interface. The top plot shows that the charge density $\rho_z = Z\rho_M + \rho_+ - \rho_-$ has a dipolar structure. Correspondingly there is a localized electric field, shown in the middle plot, and a smooth jump of $\Delta\psi \approx 20.5$ mV in the electrostatic potential, shown in the bottom plot. This is the junction potential, which can also be calculated directly from the coexisting bulk densities as in Eq. (16). This electrical structure is in accord with general expectations for charged systems [45,60,61].

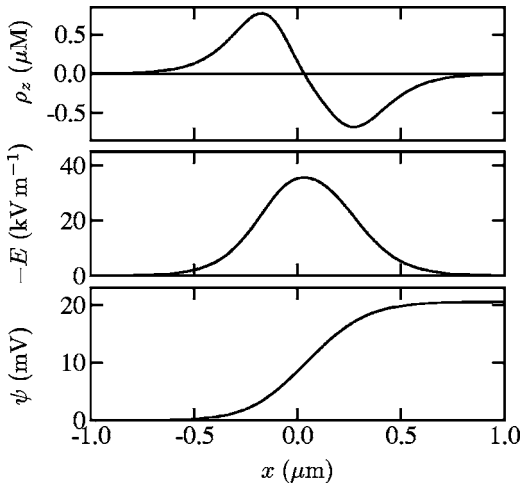

FIG. 4. Charge density (top), electric field (middle), and electrostatic potential (bottom) corresponding to the ion density profiles shown in Fig. 3.

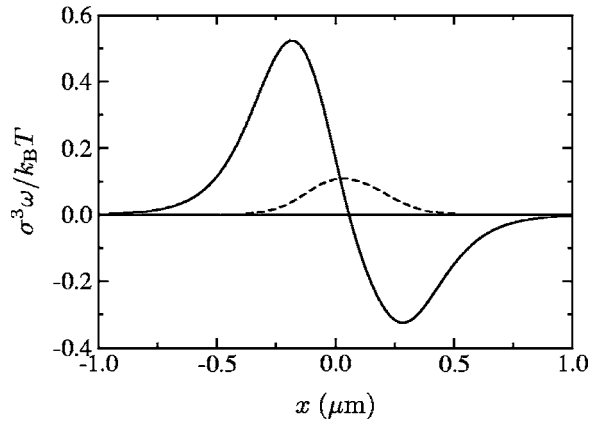

FIG. 5. Excess grand potential density (solid line) and electrostatic component thereof (dashed line) corresponding to the ion density profiles shown in Fig. 3.

Figure 5 shows the grand potential density and the electrostatic component thereof—the second term of Eq. (12)—as a function of distance through the interface. For this particular case the area gives $\gamma \approx 0.727 \times (k_B T/\sigma^2)$. The order of magnitude of this should not come as a surprise since σ and $k_B T$ are the only relevant length and energy scales in the problem. Inserting actual values, $\gamma \sim 0.3$ μN m^{-1}, which is typical for for soft matter interfaces [26,27].

Figure 6 shows how the surface tension and interface width vary as one approaches the upper critical point in Fig. 2. The width d is defined operationally as $d^2 = \langle x^2 \rangle - \langle x \rangle^2$, where $\langle \cdots \rangle = \int_{-\infty}^{\infty} (\cdots) p(x) dx / \int_{-\infty}^{\infty} p(x) dx$, with $p(x) = |\omega(x) - \omega(\pm\infty)|^2$. These results are obtained by repeating the calculations underlying Figs. 3–5 for a sequence of tie lines approaching the critical point. They are reported as a function of the distance from the critical point, expressed in terms of a normalized salt chemical potential. Figure 6(b) also shows the correlation lengths $\xi_\pm$ in the coexisting phases determined from the exponential decay of the density profiles into the bulk phases (see Appendix D). As the critical point is approached, these approach each other, and diverge in the same way as the interface width. Figure 6 reveals that the surface tension and length scales are in accord with the expected scaling behavior for a mean-field theory [62]. Last, Eq. (16) shows that the junction potential $\Delta\psi$ should vanish in proportion to the density difference, on approaching the critical point [63].

What happens at the lower critical point in Fig. 2 though? The next section shows that this is a nontrivial question with perhaps an unexpected answer. In the calculations in the present section, I have assumed that the interface profiles smoothly interpolate between the coexisting phases. Indeed, this is the basis of the numerical method detailed in Appendix D. However, such an approach rules out the possibility of oscillatory behavior in the density profiles (or to be precise,

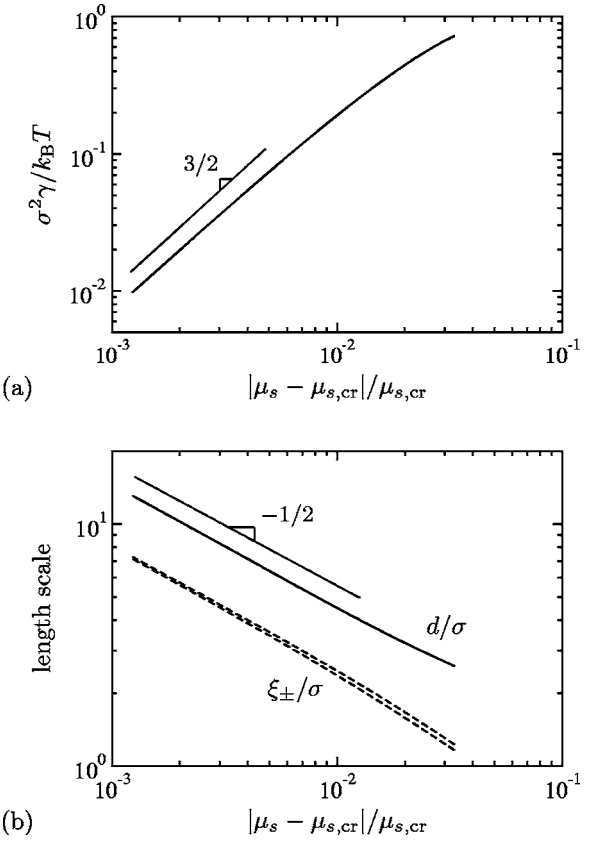

FIG. 6. (a) Surface tension as a function of salt chemical potential. (b) Interface width (solid line) and correlation lengths (dashed lines) as a function of salt chemical potential. In both, the salt chemical potential is expressed as a normalized distance from the upper critical point.

the numerical methodology is inappropriate for this scenario). At lower salt concentrations though, one can enter a region where oscillatory behavior is expected. These considerations are made mathematically precise in the next section.

V. STRUCTURE FACTORS

The structure factors in a homogeneous system can be determined from the DFT by functional differentiation [36,37]. Where accurate structure factors are already known, typically from a combination of simulation and integral equation approaches, this can be used to constrain the DFT. In the present case for example, one could try to constrain $w(r)$ in Eq. (4). However, accurate structure factors are not known for this problem, and furthermore the DFT has been constructed to include only the (linearized) macroion self-energy. Thus it does not make sense to constrain the DFT. The present section simply reports the structure factors that are predicted from the theory as given in Eqs. (1)–(4).

The structure factor matrix is [64,65]

$$\widetilde{S}_{ij}(q) = \rho_i\delta_{ij} + \rho_i\rho_j\widetilde{h}_{ij}(q) \tag{17}$$

where i and j run over $\{m,+,-\}$ and $\widetilde{h}_{ij}(q) = \int d^3\mathbf{r}\, e^{-i\mathbf{q}\cdot\mathbf{r}}h_{ij}(r)$ is the Fourier transform of the pair correlation functions $h_{ij}(r)=g_{ij}(r)-1$. Reciprocal space quantities will be denoted by a tilde. The bulk densities ρ_i are constants, fixed by the choice of state point. Deviations away from these will be denoted by $\Delta\rho_i$. Equation (17) uses the normalization $\widetilde{S}_{ij}(q)\to\rho_i\delta_{ij}$ as $q\to\infty$, which simplifies some of the expressions below [65].

To obtain the structure factor matrix, start by defining the real-space function

$$S_{ij}^{-1}(|\mathbf{r}-\mathbf{r}'|) = \frac{1}{k_BT}\left(\frac{\delta^2F}{\delta\rho_i(\mathbf{r})\,\delta\rho_j(\mathbf{r}')}\right)_{\rho_i(\mathbf{r})\to\rho_i} \tag{18}$$

where F is the full free energy. The limit of a homogeneous system is taken after the functional differentiation step so that S_{ij}^{-1} only depends on $|\mathbf{r}-\mathbf{r}'|$ as indicated. Transforming to reciprocal space, one can show that

$$\widetilde{S}_{ij}^{-1}(q) = \int d^3\mathbf{r}\, e^{-i\mathbf{q}\cdot\mathbf{r}}S_{ij}^{-1}(r) \tag{19}$$

is simply the matrix inverse of $\widetilde{S}_{ij}$,

$$\sum_j \widetilde{S}_{ij}\widetilde{S}_{jk}^{-1} = \delta_{ik}. \tag{20}$$

These results follow by combining the Ornstein-Zernike relation for a multicomponent mixture in reciprocal space, $\widetilde{h}_{ij} = \widetilde{c}_{ij} + \Sigma_k\rho_k\widetilde{c}_{ik}\widetilde{h}_{jk}$ where c_{ij} are the direct correlation functions [64], with the DFT result that $c_{ij} = -(1/k_BT)\,\delta^2F_{ex}/\delta\rho_i\delta\rho_j$ where F_{ex} is the excess free energy [36,37].

The route to the structure factors offered by Eqs. (18)–(20) is based on "classical" arguments [64]. One can also make the connection via field theoretical methods. Expanding the free energy functional to second order gives

$$\frac{\Delta F}{k_BT} = \frac{1}{2}\int d^3\mathbf{r}\, d^3\mathbf{r}' \sum_{ij}\Delta\rho_i(\mathbf{r})\Delta\rho_j(\mathbf{r}')S_{ij}^{-1}(|\mathbf{r}-\mathbf{r}'|), \tag{21}$$

where S_{ij}^{-1} is defined by Eq. (18). It follows that [66]

$$\langle\Delta\rho_i(\mathbf{r})\Delta\rho_j(\mathbf{r}')\rangle = S_{ij}(|\mathbf{r}-\mathbf{r}'|) \tag{22}$$

where $S_{ij}(r) = \int d^3\mathbf{q}/(2\pi)^3 e^{i\mathbf{q}\cdot\mathbf{r}}\widetilde{S}_{ij}(q)$ is the structure factor matrix expressed as a real-space quantity. Although care has to be taken at the point $\mathbf{r}=\mathbf{r}'$, one can easily show that the density-density correlation function on the left hand side of Eq. (22) is the same as the Fourier transform of the right hand side of Eq. (17).

The Stillinger-Lovett moment conditions constrain the behavior of the structure factors in reciprocal space in a particularly clear manner [29,30,44,67–69]. First, the zeroth-moment conditions express perfect screening and are $\int d^3\mathbf{r}\Sigma_i z_i\rho_i g_{ij}(r) = -z_j$ for $j=\{m,+,-\}$. Using charge neutrality and assuming the structure factors are regular at $q=0$, one can easily show that this implies

$$\sum_i z_i\widetilde{S}_{ij}(\mathbf{q}) = O(q^2). \tag{23}$$

The second-moment condition is $\int d^3\mathbf{r}\, r^2\Sigma_{ij}z_iz_j\rho_i\rho_j g_{ij}(r) = -3/(2\pi l_B)$. This constrains the long wavelength behavior of the charge-charge structure factor,

$$\sum_{ij} z_i z_j \tilde{S}_{ij}(\mathbf{q}) = \frac{q^2}{(4\pi l_B)} + O(q^4). \tag{24}$$

In real space, this means that $\langle \Delta\rho_z(\mathbf{r}) \Delta\rho_z(\mathbf{r}') \rangle \sim l_B / |\mathbf{r}-\mathbf{r}'|$ for $|\mathbf{r}-\mathbf{r}'| \to \infty$. Thus charge density fluctuations vanish with the Coulomb law at large distances, corresponding to the fact that the electrostatic energy dominates in the free energy for long wavelength density fluctuations unless they happen to be charge neutral [30,67,69].

I now apply the formalism of Eqs. (18)–(20) to the present DFT defined in Eqs. (1)–(4). The result for the inverse structure factor matrix in reciprocal space can be written as

$$\tilde{S}_{ij}^{-1} = \tilde{T}_{ij}^{-1} + \frac{4\pi l_B z_i z_j}{q^2} \tag{25}$$

where the first term comes from the ideal and correlation contributions to the free energy and the second term from the mean-field electrostatics. The first term is in detail

$$\tilde{T}_{ij}^{-1} = \delta_{ij}/\rho_i + \rho_m Z^2 \pi^2 l_B^3 \sigma^3 h_1(\sigma\kappa, \sigma q) \Delta'_{ij} - Z^2 \pi l_B^2 \sigma h_2(\sigma\kappa, \sigma q) \Delta''_{ij}, \tag{26}$$

where the functions $h_{1,2}(x=\sigma\kappa, y=\sigma q)$ are

$$h_1 = \frac{8e^{-\alpha y^2/2}(2+3x)}{x^3(x+2)^3}, \quad h_2 = \frac{4e^{-\alpha y^2/4}}{x(x+2)^2}, \tag{27}$$

and the matrices are

$$\Delta'_{mm} = \Delta'_{m\pm} = 0, \quad \Delta'_{\pm\pm} = 1,$$

$$\Delta''_{mm} = \Delta''_{\pm\pm} = 0, \quad \Delta''_{m\pm} = 1. \tag{28}$$

The y dependence ($y=\sigma q$) in Eq. (27) arises from the Fourier transform of the weight function of Eq. (4). Note here that the point model alluded to in Sec. II corresponds to the limit $\alpha \to 0$ in Eqs. (27). In this limit, the theory becomes unphysical since $\tilde{S}_{ij}(q)$ does not have the correct limiting behavior as $q \to \infty$. This provides a strong technical motivation for introducing a smoothing kernel.

For any given state point and value of q, Eqs. (25)–(28) define $\tilde{S}_{ij}^{-1}$ which can be inverted numerically to find all components of the structure factor matrix. A partial solution can be obtained analytically in terms of the subsidiary matrix $\tilde{T}_{ij}$,

$$\tilde{S}_{ij} = \tilde{T}_{ij} - \frac{4\pi l_B \sum_{kl} z_k z_l \tilde{T}_{ik} \tilde{T}_{jl}}{q^2 + 4\pi l_B \sum_{kl} z_k z_l \tilde{T}_{kl}}. \tag{29}$$

From this one can readily prove that $\tilde{S}_{ij}$ satisfies all the Stillinger-Lovett moment conditions exactly, as in Eqs. (23) and (24) above.

Another result follows from the dominance of the ideal contribution over the correlation contribution at low densities. In the limit $\rho_i \to 0$ one finds $\tilde{T}_{ij} \to \rho_i \delta_{ij}$ and

$$\tilde{S}_{ij} \to \rho_i \delta_{ij} - \frac{4\pi l_B z_i z_j \rho_i \rho_j}{q^2 + 4\pi l_B \sum_k z_k^2 \rho_k}. \tag{30}$$

This is in fact exactly in accordance with the Debye-Hückel limiting law at low densities. To see this, note that $\lambda = (4\pi l_B \Sigma_k z_k^2 \rho_k)^{-1/2}$ is the Debye screening length defined to include *all* ionic species. Thus in real space, Eqs. (17) and (30) indicate that $h_{ij} = -z_i z_j (l_B/r) e^{-r/\lambda}$, in correspondence with the Debye-Hückel limiting law.

It is clear that the moment conditions and the Debye-Hückel limiting law behavior follow from the construction of the DFT to include a mean-field contribution separately from the correlation term. This construction is in turn motivated by the expected behavior of the direct correlation functions $c_{ij}(r)$ at $r \to \infty$, as Evans and Sluckin have described [44]. The form of the correlation term is unimportant, so long as it is regular at both $q \to 0$ and $\rho_i \to 0$. Thus a DFT approach to charged systems incorporates automatically a degree of internal consistency, although yet further requirements could be imposed [70].

For the remaining part, I now focus on the macroion structure factor $\tilde{S}_{mm}$. Note that the theory includes the macroion-macroion electrostatic interaction explicitly in the mean-field term, and an additional indirect interaction in the correlation term. The computation of $\tilde{S}_{mm}$ reveals the combined effect of these macroion interactions on the macroion correlations.

Typically $\tilde{S}_{mm}$ has a "hole" in reciprocal space for $q\sigma \lesssim 1$. This corresponds to the macroion electrostatic repulsions. Within the correlation hole though, there is additional structure. This becomes particularly important in the vicinity of the phase separation region. Two kinds of behavior are possible: at higher salt concentrations $\tilde{S}_{mm}$ rises to a maximum as $q \to 0$, or at lower salt concentrations $\tilde{S}_{mm}$ acquires a peak at some $q^* > 0$. In the phase diagram, the two alternatives are separated by a (macroion) "Lifshitz line" [71], defined to be the locus of points for which $\partial \tilde{S}_{mm} / \partial (q^2)|_{q=0} = 0$. Figure 7(a) shows the two behaviors for a pair of typical state points above and below the Lifshitz line, and Fig. 7(b) shows the Lifshitz line superimposed on the bulk phase behavior.

Also shown in Fig. 7(b) is the spinodal line computed from the bulk free energy in Eq. (5) of Sec. III. One can check that $\tilde{S}_{mm}(q=0)$ diverges on this spinodal line; in fact all the $q=0$ components of the structure factor matrix diverge because the determinant of $\tilde{S}_{ij}^{-1}$ vanishes. For salt concentrations above the Lifshitz line, this divergence at $q=0$ can be accommodated within the general behavior of the structure factor. Of course, state points within the binodal are metastable so the divergence is strictly only visible as the upper critical point is approached. The fact that the structure factors diverge on the spinodal line is no coincidence, since thermodynamic consistency by the compressibility route is assured for a DFT [72].

What happens at salt concentrations below the Lifshitz line? Here, the peak in S_{mm} at $q^* > 0$ is found to diverge

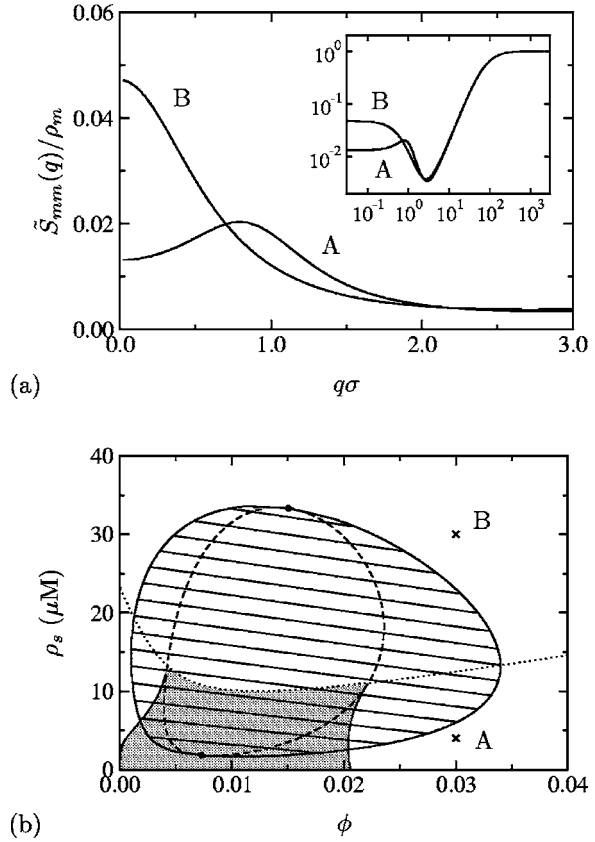

FIG. 7. (a) Macroion structure factors at $\phi=0.03$, and $\rho_s=4$ (A) and 30 μM (B). The inset shows the same curves in a double-logarithmic plot. The normalization is such that $\tilde{S}_{mm}/\rho_m \to 1$ as $q \to \infty$. (b) Phase diagram augmented by the spinodal line (dashed), the Lifshitz line (dotted), and the region where the macroion structure factor diverges at a nonzero wave vector (shaded).

before the bulk spinodal line is reached. The shaded area in Fig. 7(b) shows the region where this occurs. A divergence at a nonzero wave vector is indicative of microphase separation [73,74]. In this case one would expect a charge density wave (CDW) phase to appear [32,75]. The shaded region extends below the binodal for bulk phase separation, so the CDW phase should be observable in this part of the phase diagram. In fact the CDW phase will be found whenever the lower critical point lies below the Lifshitz line. The general idea that a critical point in a charged system can be replaced by a CDW phase was advanced by Nabutovskii, Nemov, and Peisakhovich [32].

The location of the Lifshitz line depends on the parameter α which sets the range of the smoothing kernel $w(r)$ in Eq. (4). If $\alpha \lesssim 0.40$ the Lifshitz line moves upward past the upper critical point, which would then be expected to be replaced by a CDW phase too. On the other hand if $\alpha \gtrsim 3.6$, the Lifshitz line moves downward past the lower critical point. These critical values of α depend only on the coefficient of q^2 in the expansion of the Fourier transform of $w(r)$ about $q=0$.

The Lifshitz line discussed here pertains to the macroion structure factor. Although slightly different Lifshitz lines are expected for each component of the structure factor matrix, the locus of state points where the peak diverges (either on the spinodal or on the boundary of the CDW phase) should be the same for all components.

While the Lifshitz line marks an obvious change in the behavior of $\tilde{S}_{mm}$, the crossover from monotonic to damped oscillatory asymptotic decay of the correlation functions $h_{ij}(r)$ is determined by Kirkwood or Fisher-Widom lines in the phase diagram [76–79]. The difference between these is rather subtle [79,80], and one might loosely cover both possibilities by the phrase "Kirkwood-Fisher-Widom" (KFW) line. The importance of the KFW line lies in the fact that it also governs the asymptotic decay of the interface density profiles, which behave in the same way as h_{ij} [78]. Thus the calculations reported in Sec. IV, which assume that there is no oscillatory behavior in the density profiles, requires as a necessary minimum that the coexisting bulk densities both lie above the KFW line. The location of the KFW line is governed by the poles of $\tilde{S}_{ij}(q)$ in the complex q plane, which either are purely imaginary or occur as complex conjugate pairs, and are the same for all components of $\tilde{S}_{ij}$ [78]. If the pole nearest the real q axis is purely imaginary, then monotonic decay is expected; conversely if a pair of complex conjugate poles is nearest the real q axis, then damped oscillatory decay is expected [79]. Determination of the KFW line is a hard numerical problem and has not been attempted for the present DFT. However, the presence of a peak in $\tilde{S}_{mm}(q)$ on the real q axis at $q=0$, or at $q^* > 0$, ought to be indicative of whether the pole nearest the real q axis is, or is not, purely imaginary. Thus the Lifshitz line should serve as a guide to the location of the KFW line. In Sec. IV therefore, care was taken to make sure that the coexisting bulk densities lie well above the Lifshitz line.

VI. DISCUSSION

The paper presents a density functional theory for a macroion suspension. The correlation free energy corresponds to the macroion self-energy evaluated using Debye-Hückel theory. These approximations render the theory tractable without losing the basic phenomenology which resembles that of other studies. The macroion self-energy depends on the local ionic strength, but on both physical and technical grounds it is found necessary to introduce the notion of smoothing or smearing, so that the self-energy depends on the ionic strength averaged over the vicinity of the macroion. Here a completely phenomenological approach has been taken to construct the details of the DFT. Other choices could be made, or indeed more rigor could be introduced. Tests indicate though that the general phenomenology (interface structure, gross behavior of structure factors) is insensitive to the details of the model at this point.

The advantage of a DFT is that one can compute the interface structure and surface tension between coexisting phase. The results are in accord with expectations from previous work [11,26–28]. In particular, the electrical structure of the interface gives rise to a junction potential analogous to the Donnan potential across a semipermeable membrane. This arises from an electric dipole moment density (per unit

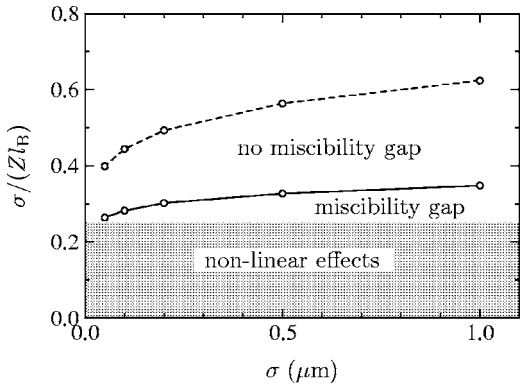

FIG. 8. State diagram showing where a miscibility gap is found for the full theory of Ref. [11] including the omitted term (solid line), compared to the original results (dashed line). The shaded region shows where $Z \gtrsim 4\sigma/l_B$, which is one possible criterion for the acceptability of the Debye-Hückel approximation for the polarization energy [11].

area of interface), which appears because charge neutrality is locally violated in the vicinity of the interface. The surface tension is found to be of the order k_BT/σ^2.

Structure factors can be computed from the DFT. These are found to obey the Stillinger-Lovett moment conditions, although this is not a stringent test of the theory. The structure factors reveal an interesting phenomenon, namely, that oscillatory behavior can appear in the (direct) correlation functions, particularly at low ionic strength. Indeed the structure factors may be found to diverge at a nonzero wave vector on approaching the critical points, indicating that the critical point(s) may be replaced by regions of microphase separation corresponding to the appearance of a charge density wave phase. This phenomenon is peculiar to asymmetric charged systems [32], and is strictly absent in symmetric systems such as the restricted primitive model. In this respect, the possibility of CDW phases is correlated with the appearance of the junction potential, which is also strictly absent in symmetric systems [31].

Given the approximate nature of the DFT, only certain aspects of the present analysis might be expected to survive in a full treatment. One of these is an upturn in macroion structure factor at small q, even in the absence of a true miscibility gap. This would reflect an increased osmotic compressibility in this region of the phase diagram. This conclusion ought to be robust, since it does not require that Zl_B/σ be so large as to stray into the nonlinear region.

Another expectation is the possible appearance of the CDW phases. By analogy to the calculations for polyelectrolytes [73,74] one might expect these to resemble liquid crystal mesophases (lamellar phase, etc.) in the vicinity of the critical points. Away from the critical points though, the structures that form might resemble micellar systems. For example, at low macroion densities, an equilibrium population of macroion aggregates might appear. This is not a hypothetical possibility, since there is good evidence for the appearance of equilibrium clusters in protein solutions and colloidal suspensions [81]. The phenomenon in those systems is attributed to the presence of attractive forces which are shorter in range than the electrostatic repulsive forces [82,83]. However, essentially the same mechanism is in operation in the present DFT, where the attractive forces correspond to the correlation term and are of range σ, and the repulsive forces correspond to the mean-field electrostatic term and are of infinite range. Interestingly, the simulations of Linse *could* be interpreted as supporting the idea of the appearance of a "micellar" aggregate phase before the bulk phase instability. The published simulation snapshots do appear to show macroion clusters [Fig. 8(b) in Ref. [8]] and the corresponding macroion-macroion pair distribution function acquires a peak at contact which could be interpreted as being due to macroions in clusters (Fig. 5 in Ref. [8]). Whether this is actually the case or not must remain a subject for future investigations.

ACKNOWLEDGMENTS

I thank R. Evans and A. S. Ferrante for useful discussions.

APPENDIX A: CORRECTION TO REF. [11]

Chan [84] has remarked that an excluded volume contribution was omitted in the theory of Ref. [11]. This appendix describes the missing term. The error occurs in going from Eq. (3) to Eq. (7) of Ref. [11] where the omitted contribution arises from the fact that $h_{m\pm}(r)=g_{m\pm}(r)-1=-1$ for $r<\sigma/2$. In terms of the small ion–macroion interaction energy, $E_{ms}/(Vk_BT)$, the omitted contribution is

$$\rho_m \int_{|\mathbf{r}|<\sigma/2} d^3\mathbf{r} \frac{Zl_B}{r}[\rho_+ h_{m+}(r) - \rho_- h_{m-}(r)] = \frac{\pi Z^2 l_B \rho_m^2 \sigma^2}{2}. \tag{A1}$$

This contribution passes unscathed through the thermodynamic integration step needed to calculate the contribution to the free energy because it is an athermal excluded volume term. It is a positive, increasing function of ρ_m and has the tendency to stabilize the system against phase separation. If the calculations of Ref. [11] are repeated with this contribution included, it is found that the basic phenomenology is still the same, except that the miscibility gap in the (ρ_m, ρ_s) plane does not appear until somewhat larger values of Zl_B/σ. Figure 8 shows the new results in comparison with those reported in Table II of Ref. [11].

The new calculation indicates that phase separation is observed in an even more marginal window of admissible parameter space than was found in the earlier work. Thus one can conclude that, to explain phase separation, some other physics is likely to be required in addition to that captured in the theory in Ref. [11]. This conclusion is now much closer to the Poisson-Boltzmann cell model calculations which show that phase separation in a cell model is a consequence of the linearization approximation [17–19].

APPENDIX B: SIGNIFICANCE OF SELF-ENERGY

The discussion at the end of the previous Appendix and Fig. 8 both indicate that the self-energy is still important for

this problem. This is supported by the calculation in the main text which shows that phase separation can be driven by the self-energy term alone for $Zl_B/\sigma \gtrsim 6.89$ (i.e., at the hypercritical point in the presence of salt for $Z=10^3$), which is not far above saturating value of the effective charge $Z_{\mathrm{eff}} l_B/\sigma \approx 4$ [8,12].

To refine the analysis, consider the problem in the absence of added salt. The inverse compressibility from Eq. (6) is

$$\frac{1}{k_B T}\frac{\partial p}{\partial \rho} = Z - \frac{3Z^2 l_B(\sqrt{6u}+2u)}{4\sigma(\sqrt{6u}+1)^3} \tag{B1}$$

where $u=\phi Z l_B/\sigma$. The first term is the ideal term (dominated by the counterions) and the second term is the contribution of the self-energy term. The second term is always negative, and therefore tends to destabilize the system. This observation can be placed on a tighter numerical footing though. The critical point for the system studied by Reščič and Linse [10] is at $\phi \approx 0.15$ and $\sigma/l_B \approx 2/2.6=0.77$ (in their notation, $\Gamma_{II} = 2l_B/\sigma \propto 1/T$). Making a conservative estimate by replacing Z by $Z_{\mathrm{eff}}=4\sigma/l_B \approx 3.1$ in the above, the contribution of the self-energy term to the inverse compressibility at the critical point is ≈ -1.17, in other words $1.17/3.1 \approx 40\%$ of the ideal term at the state point in question (only the free counterions are supposed to contribute to the free term). One can also try to compare with the actual compressibility. From Fig. 4(b) of Ref. [10], one can estimate the slope of the $p(\rho_m)$ curve at a temperature slightly below the critical point. Thus, at $\sigma/l_B \approx 2/2.846=0.703$, the turning points of $p(\rho_m)$ are at $(pR_m^3/k_BT, \rho_m R_m^3) \approx (0.002\,53, 1/27.)$ and $(0.002\,98, 1/34.)$. From this, $(1/k_BT)\partial p/\partial \rho_m \approx (0.002\,53-0.002\,98)/(1/27-1/34) = -0.059$. Now, one expects the inverse compressibility to scale as $(1/k_BT)\partial p/\partial \rho_m \approx A|T/T_c - 1|^{\gamma}$ in the vicinity of T_c where $\gamma \approx 1.24$ is the compressibility exponent [62]. Matching to the estimate just made therefore, the prefactor in the inverse compressibility scaling law is estimated to be $A \approx 0.059 \times |0.703/0.77 - 1|^{-\gamma} = 1.2$. This should be compared to the self-energy contribution to the inverse compressibility estimated above (-1.17 at the critical point). The comparison suggests that the self-energy contribution should be important for a significant range of temperatures around the critical point.

APPENDIX C: SMALL ION SUBSYSTEM

It is often assumed that the size of the small ions should be unimportant for the problem of the phase behavior of macroion suspensions. However this statement requires some caution, as I now discuss. As Onsager remarked a long time ago [85], one cannot strictly set the small ion size to zero. In fact the problem is more serious than this because the small ion subsystem becomes increasingly nonideal as the ion size is decreased. To make this concrete, imagine that the small ion subsystem is modeled by the restricted primitive model (RPM). The RPM has a critical point at a reduced temperature $\sigma_s/l_B \approx 0.050$ [86], where σ_s is the small ion diameter. To be treated as ideal, one should therefore require $\sigma_s/l_B \gg 0.050$. The question is, can this be made consistent with the phase behavior of the macroion plus small ion system?

If one takes $\sigma/(Zl_B) \approx 0.14$ as characteristic of the reduced temperature at which the macroion system shows interesting phase behavior (see Fig. 1 for instance), then the above condition becomes $Z\sigma_s/\sigma \gg 0.050/0.14 \approx 0.35$ or $Z \gg 0.35(\sigma/\sigma_s)$. This means that the calculations in the main text are safe (take for example $\sigma_s=1$ nm; then $Z \gg 35$ is required for $\sigma=100$ nm). Moreover, since $Z \sim \sigma^2$ might be expected for macroions at constant surface charge density, one can always satisfy the inequality by making σ sufficiently large.

By way of contrast, the simulations reported by Hynninen, Dijkstra, and Panagiotopoulos [54] have the small ion critical point at a higher temperature than the macroion plus small ion system. Thus it is not obvious that their results are immediately applicable to the present problem of the phase behavior of macroion suspensions where the supporting electrolyte can be assumed to be ideal. This might also be the reason why a qualitatively different effect of added salt on the macroion critical point is seen in these simulations, compared to theoretical calculations [11,20,21,39,40,53] (and the present one; it should nevertheless be stressed that the theoretical calculations involve approximations which may be wrong).

APPENDIX D: NUMERICAL APPROACH

The task is to find density profiles $\rho_i(x)$ that minimize the grand potential in Eq. (7). The most accurate method is to solve the integral equations for the profiles in Eq. (13), together with the Poisson equation. However, this is hard. An alternative is to adopt a variational approach in which γ is minimized with respect to parameters in trial functions which specify the density profiles [87,88]. This is the approach that has been taken here. Note that γ is the difference between Ω for the inhomogeneous problem and Ω in a coexisting homogeneous system, therefore minimizing γ is equivalent to minimizing Ω.

The ion density profiles have to satisfy a sum rule since the potential difference $\Delta\psi = \psi(\infty) - \psi(-\infty)$ is fixed by the coexisting bulk densities as described in Sec. III. One can replace one of the ion density profiles by $\psi(x)$ to ensure this sum rule is automatically satisfied. In the present case, a choice was made to use the set $\{\rho_m, \rho_+, \psi\}$ as a basis, with ρ_- derived analytically from the Poisson equation $\rho_- = Z\rho_m + \rho_- - (d^2\psi/dx^2)/(4\pi l_B)$. The first integral of the Poisson equation shows that one can additionally ensure global charge neutrality by making sure that $d\psi/dx \to 0$ as $|x| \to \infty$. Once the ρ_i are known, the average ionic strength $\bar{\rho}_I$ and the surface tension γ are determined numerically by quadratures.

To represent the basis set $\{\rho_m, \rho_+, \psi\}$, three copies of the function

$$f(x;\xi_\pm, a_\pm, a_r) = \frac{a_- e^{x/\xi_+} - a_+ e^{-x/\xi_-}}{a_- a_+ + a_- e^{x/\xi_+} + a_+ e^{-x/\xi_-}} + \sum_{r=1}^{N} a_r H_r(x/\xi) \tag{D1}$$

are introduced. In this, the H_r are Hermite functions, with $\xi = 2/(1/\xi_- + 1/\xi_+)$ used to scale the argument. Each copy of

f is parametrized by the correlation lengths $\xi_\pm$ and amplitude set $\{a_\pm, a_r\}$, and has the properties that $f \to \pm(1-a_\pm e^{\mp x/\xi_\pm})$ as $x \to \pm\infty$. One copy of f is assigned to each member of $\{\rho_m, \rho_+, \psi\}$, and is scaled and shifted to match the limiting values at $x \to \pm\infty$, for example $\rho_m = \rho_m(-\infty)(1-f)/2 + \rho_m(\infty)(1+f)/2$ [for the electrostatic potential, one sets $\psi(-\infty)=0$ and $\psi(\infty)=\Delta\psi$ as explained in the main text]. The three copies of f have different amplitude sets $\{a_\pm, a_r\}$ but share common values for $\xi_\pm$ since the asymptotic decay of the density profiles into the bulk phases is expected to be governed by the bulk correlation length (it is these values of $\xi_\pm$ that are reported in Fig. 6). A finite set of N Hermite functions has been included in each copy of f to allow for an arbitrary structure at the interface. In practice the minimization problem is well behaved only if the density profiles smoothly interpolate between the bulk values, for which case typically $N=3-6$ Hermite functions achieve convergence in γ to an accuracy of the order 1%. At this point, the interface problem has been reduced to a multivariate minimization over the three copies of the amplitude set $\{a_\pm, a_r\}$, plus the correlation lengths $\xi_\pm$. Numerical minimization of γ with respect to these parameters is then undertaken by standard methods [89].

[1] A. K. Akora and B. V. R. Tata, Adv. Colloid Interface Sci. **78**, 49 (1998).
[2] J.-P. Hansen and H. Löwen, Annu. Rev. Phys. Chem. **51**, 209 (2000).
[3] C. N. Likos, Phys. Rep. **348**, 267 (2001).
[4] Y. Levin, Rep. Prog. Phys. **65**, 1577 (2002).
[5] L. Belloni, J. Phys.: Condens. Matter **12**, R549 (2000).
[6] P. Linse and V. Lobaskin, Phys. Rev. Lett. **83**, 4208 (1999).
[7] P. Linse and V. Lobaskin, J. Chem. Phys. **112**, 3917 (2000).
[8] P. Linse, J. Chem. Phys. **113**, 4359 (2000).
[9] V. Lobaskin and K. Qamhieh, J. Phys. Chem. B **107**, 8022 (2003).
[10] J. Reščič and P. Linse, J. Chem. Phys. **114**, 10131 (2001).
[11] P. B. Warren, J. Chem. Phys. **112**, 4683 (2000).
[12] S. Alexander, P. M. Chaikin, G. J. Morales, P. Pincus, and D. Hone, J. Chem. Phys. **80**, 5776 (1984).
[13] R. D. Groot, J. Chem. Phys. **95**, 9191 (1991).
[14] L. Belloni, Colloids Surf., A **140**, 227 (1998).
[15] E. Trizac, L. Bocquet, and M. Aubouy, Phys. Rev. Lett. **89**, 248301 (2002).
[16] L. Bocquet, E. Trizac, and M. Aubouy, J. Chem. Phys. **117**, 8138 (2002).
[17] H. H. von Grünberg, R. van Roij, and G. Klein, Europhys. Lett. **55**, 580 (2001).
[18] M. Deserno and H. H. von Grünberg, Phys. Rev. E **66**, 011401 (2002).
[19] M. N. Tamashiro and H. Schiessel, J. Chem. Phys. **119**, 1855 (2003).
[20] A. Diehl, M. C. Barbosa, and Y. Levin, Europhys. Lett. **53**, 86 (2001).
[21] J.-F. Dufrêche, T. O. White, and J.-P. Hansen, Mol. Phys. **101**, 1741 (2003).
[22] Y. Levin, E. Trizac, and L. Bocquet, J. Phys.: Condens. Matter **15**, S3523 (2003).
[23] E. Trizac and Y. Levin, Phys. Rev. E **69**, 031403 (2004).
[24] K. S. Schmitz, Langmuir **13**, 5849 (1997).
[25] F. Gröhn and M. Antonietti, Macromolecules **33**, 5938 (2000).
[26] J. M. Brader and R. Evans, Europhys. Lett. **49**, 678 (2000).
[27] E. Scholten, R. Tuinier, R. H. Tromp, and H. N. W. Lekkerkerker, Langmuir **18**, 2234 (2002).
[28] P. B. Warren, J. Phys.: Condens. Matter **15**, S3467 (2003).
[29] F. H. Stillinger and R. Lovett, J. Chem. Phys. **49**, 1991 (1968).
[30] P. A. Martin, Rev. Mod. Phys. **60**, 1075 (1988).
[31] P. B. Warren, e-print cond-mat/0006289.
[32] V. M. Nabutovskii, N. A. Nemov, and Y. G. Peisakhovich, Phys. Lett. **79A**, 98 (1980).
[33] J. S. Hoye and G. Stell, J. Phys. Chem. **94**, 7899 (1990).
[34] M. E. Fisher, J. Stat. Phys. **75**, 1 (1994).
[35] M. Knott and I. J. Ford, Phys. Rev. E **65**, 061401 (2002).
[36] R. Evans, Adv. Phys. **28**, 143 (1979).
[37] R. Evans, in *Fundamentals of Inhomogeneous Fluids*, edited by D. Henderson (Marcel Dekker, New York, 1992), Chap. 3.
[38] E. B. Smith, *Basic Chemical Thermodynamics* (Clarendon, Oxford, 1990).
[39] R. van Roij and J.-P. Hansen, Phys. Rev. Lett. **79**, 3082 (1997).
[40] R. van Roij, M. Dijkstra, and J.-P. Hansen, Phys. Rev. E **59**, 2010 (1999).
[41] B. Beresford-Smith, D. Y. Chan, and D. J. Mitchell, J. Colloid Interface Sci. **105**, 216 (1985).
[42] More complicated expressions for the self-energy are available [11], but it has been checked that the use of these does not alter the basic phenomenology.
[43] It has been checked that the phenomenology is robust with respect to the choice of $w(r)$.
[44] R. Evans and T. J. Sluckin, Mol. Phys. **40**, 413 (1980).
[45] T. J. Sluckin, J. Chem. Soc., Faraday Trans. 2 **77**, 1029 (1981).
[46] R. Evans and M. Hasegawa, J. Phys. C **14**, 5225 (1981).
[47] M. J. Stevens and M. O. Robbins, Europhys. Lett. **12**, 81 (1990).
[48] C. N. Patra and S. K. Ghosh, Phys. Rev. E **48**, 1154 (1993).
[49] P. B. Warren, J. Phys. II **7**, 343 (1997).
[50] E. González-Tovar, Mol. Phys. **97**, 1203 (1999).
[51] L. B. Bhuiyan and C. W. Outhwaite, J. Chem. Phys. **116**, 2650 (2002).
[52] Note the approximate constancy of $Z\Gamma = 2Zl_B/\sigma$ at the critical points in Table V of Ref. [51].
[53] S. N. Petris and D. Y. C. Chan, J. Chem. Phys. **116**, 8588 (2002).
[54] A.-P. Hynninen, M. Dijkstra, and A. Z. Panagiotopoulos, J. Chem. Phys. **123**, 084903 (2005).
[55] J. S. Walker and C. A. Vause, J. Chem. Phys. **79**, 2660 (1983).
[56] F. A. Hinchey, *Introduction to Applicable Mathematics* (Wiley Eastern, New Delhi, 1980).
[57] Equation (9) limits to $\psi\rho_z/2$ which is different from Eq. (5). This is because the constraint term in Eq. (5) is inserted by

hand and does not correspond to a charging process. The difficulty is more apparent than real though, since it disappears when the chemical potentials are computed.
[58] F. G. Donnan, Z. Elektrochem. Angew. Phys. Chem. **17**, 572 (1911).
[59] J. T. G. Overbeek, J. Colloid Sci. **8**, 593 (1953).
[60] V. M. Nabutovskii and N. A. Nemov, J. Colloid Interface Sci. **114**, 208 (1986).
[61] B. Groh, R. Evans, and S. Dietrich, Phys. Rev. E **57**, 6944 (1998).
[62] J. S. Rowlinson and B. Widom, *Molecular Theory of Capillarity* (Clarendon, Oxford, 1989).
[63] I. Iosilevski and A. Chigvintsev, J. Phys. IV **10**, 451 (2000).
[64] J.-P. Hansen and I. A. McDonald, *Theory of Simple Liquids* (Academic, New York, 1976).
[65] N. H. March and M. P. Tosi, *Atomic Dynamics in Liquids* (Macmillan, London, 1976).
[66] M. Doi and S. F. Edwards, *The Theory of Polymer Dynamics* (Clarendon, Oxford, 1986).
[67] J. Stafiej and J. P. Badiali, J. Chem. Phys. **106**, 8579 (1997).
[68] B. P. Lee and M. E. Fisher, Europhys. Lett. **39**, 611 (1997).
[69] J.-N. Aqua and M. E. Fisher, Phys. Rev. Lett. **92**, 135702 (2004).
[70] For example, it has not been checked that $g_{ij}(r) \geqslant 0$. Also, one could require that the $g_{ij}(r)$ computed from the structure factors are the same as those that can be computed by solving the inhomogeneous problem of the density profiles in an appropriately chosen external potential [36,37]. Such requirements would introduce additional numerical complexity into the problem though.
[71] A. J. Archer, C. N. Likos, and R. Evans, J. Phys.: Condens. Matter **14**, 12031 (2002).
[72] One would not expect consistency by the energy or virial routes because these invoke the pair potentials. While the pair potentials are of course specified in the primitive model, the DFT itself is approximate.
[73] V. Y. Borue and I. Y. Erukhimovich, Macromolecules **21**, 3240 (1988).
[74] J. F. Joanny and L. Leibler, J. Phys. (France) **51**, 545 (1990).
[75] V. M. Nabutovskii, N. A. Nemov, and Y. G. Peisakhovich, Mol. Phys. **54**, 979 (1985).
[76] J. G. Kirkwood, Chem. Rev. (Washington, D.C.) **19**, 275 (1936).
[77] M. E. Fisher and B. Widom, J. Chem. Phys. **50**, 3756 (1969).
[78] R. Evans, R. J. F. Leote de Carvalho, J. R. Henderson, and D. C. Hoyle, J. Chem. Phys. **100**, 591 (1994).
[79] R. J. F. Leote de Carvalho and R. Evans, Mol. Phys. **83**, 619 (1994).
[80] Roughly, the period of the oscillations diverges as one approaches a Kirkwood line, but not as one approaches a Fisher-Widom line [79].
[81] A. Stradner, H. Sedgwick, F. Cardinaux, W. C. K. Poon, S. U. Egelhaaf, and P. Schurtenberger, Nature (London) **432**, 492 (2004).
[82] J. Groenewold and W. K. Kegel, J. Phys. Chem. B **105**, 11702 (2001).
[83] F. Sciortino, S. Mossa, E. Zaccarelli, and P. Tartaglia, Phys. Rev. Lett. **93**, 055701 (2004).
[84] D. Y. C. Chan, Phys. Rev. E **63**, 061806 (2001).
[85] L. Onsager, J. Phys. Chem. **43**, 189 (1939).
[86] E. Luijten, M. E. Fisher, and A. Z. Panagiotopoulos, Phys. Rev. Lett. **88**, 185701 (2002).
[87] J. R. Smith, Phys. Rev. **181**, 522 (1969).
[88] L. Orosz, Phys. Rev. B **37**, 6490 (1988).
[89] W. H. Press, B. P. Flannery, S. A. Teukolsky, and W. T. Vetterling, *Numerical Recipes* (Cambridge University Press, Cambridge, U.K., 1989).